Fermi surfaces and energy gaps in Sn/Ge(111)

TOPICAL REVIEW

Fermi surfaces and energy gaps in Sn/Ge(111)

T-C Chiang[1,2]**, M Y Chou**[3]**, T Kidd**[1,2] **and T Miller**[1,2]

[1] Department of Physics, University of Illinois at Urbana-Champaign, 1110 West Green Street, Urbana, IL 61801-3080, USA
[2] Frederick Seitz Materials Research Laboratory, University of Illinois at Urbana-Champaign, 104 South Goodwin Avenue, Urbana, IL 61801-2902, USA
[3] School of Physics, Georgia Institute of Technology, Atlanta, GA 30332-0430, USA

Abstract
One third of a monolayer of Sn adsorbed on Ge(111) undergoes a broad phase transition upon cooling from a $(\sqrt{3} \times \sqrt{3})$R30° normal phase at room temperature to a (3×3) phase at low temperatures. Since band-structure calculations for the ideal $(\sqrt{3} \times \sqrt{3})$R30° phase show no Fermi-surface nesting, the underlying mechanism for this transition has been a subject of much debate. Evidently, defects formed by Ge substitution for Sn in the adlayer, at a concentration of just a few percent, play a key role in this complex phase transition. Surface areas near these defects are pinned to form (3×3) patches above the transition temperature. Angle-resolved photoemission is employed to examine the temperature-dependent band structure, and the results show an extended gap forming in k-space as a result of band splitting at low temperatures. On account of the fact that the room temperature phase is actually a mixture of $(\sqrt{3} \times \sqrt{3})$R30° areas and defect-pinned (3×3) areas, the band structure for the pure $(\sqrt{3} \times \sqrt{3})$R30° phase is extracted by a difference-spectrum method. The results are in excellent agreement with band calculations. The mechanism for the (3×3) transition is discussed in terms of a response function and a tight-binding cluster calculation. A narrow bandwidth and a small group velocity near the Fermi surface render the system highly sensitive to surface perturbations, and formation of the (3×3) phase is shown to involve a Peierls-like lattice distortion mediated by defect doping. Included in the discussion, where appropriate, are dynamic effects and many-body effects that have been previously proposed as possible mechanisms for the phase transition.

(Some figures in this article are in colour only in the electronic version)

1. Introduction

The adsorbate system of 1/3 ML (monolayer) of Sn on Ge(111) has attracted much interest because it exhibits a rather unusual phase transition [1–6]. Diffraction from this surface shows

a $(\sqrt{3} \times \sqrt{3})$R30° reconstruction at room temperature. As the sample temperature is lowered below ∼210 K, this normal phase transforms gradually and becomes a fully developed (3×3) phase below ∼100 K, as shown by both low-energy electron diffraction and scanning tunnelling microscopy (STM). This was originally attributed to a charge-density-wave (CDW) transition, and the usual picture of electron–phonon coupling involving Fermi-surface nesting was invoked as the mechanism for the transition. However, later experimental and theoretical results have cast doubt on this simple picture, and other interpretations have been proposed. The subject remains controversial to date, and it is perhaps surprising that for such a seemingly simple system, modern techniques have not yet provided a complete understanding and agreement on the structure and properties.

Looking closely, the system is actually not quite that simple. It exhibits the same characteristics as the so-called 'complex' systems [7], as typified by many high-temperature superconductors, colossal-magnetoresistive materials, ferroelectrics, etc; namely, inhomogeneities and phase mixtures are intrinsic and important features of the phase transition [6, 8]. Many surface science techniques yield spatially averaged information, and therefore the results can be easily misinterpreted if spatial variations are neglected. The dynamic behaviour of the system also poses an interesting question. In addition to the usual phonons corresponding to harmonic lattice vibrations, the system could have more complicated potential curves or significant polaronic coupling giving rise to 'fluctuations' or time-dependent spatial features that can affect various measurements. Furthermore, one can imagine that many-body effects including magnetic ground states may be operative here. The truth is that many of the mechanisms proposed for this system regarding the 'unconventional behaviour' are extremely difficult to verify or disprove beyond doubt, and therefore, the controversy could and is likely to continue.

Such problems are well known for the complex oxides. Sn on Ge, being a binary system and easily accessible with surface science tools, is still much simpler to analyse than the complex oxides. A detailed examination of this 'model complex system' can be extremely valuable for a basic understanding of the physics of complex systems in general. A binary system almost always exhibits some degree of intermixing. This is especially so at surfaces. Sn on Ge is no exception. While Sn and Ge are nominally mutually insoluble at room temperature, STM has shown that the Sn adlayer contains a few percent of Ge admixture [1–4, 6]. For most adsorbate systems, such a small amount of admixture does not yield any noticeable effects. The Sn/Ge case is different. The 'Ge defects' can act as pinning centres, resulting in a mixed phase. Furthermore, there appears yet another subtle transition at low temperatures involving partial ordering of the Ge defects [6]. Similar chemical disorder or order effects have been seen in many complex oxides.

This paper is a review of recent results with a focus on the temperature-dependent electronic structure as measured by means of angle-resolved photoemission. Clues regarding the mechanism of a phase transition are often found in the band structure near the Fermi level (assuming that band structure remains a valid and useful concept for this system). Of primary interest here is the Fermi surface and its changes as a function of temperature. An issue of importance is whether or not the system exhibits a gap, as gap opening is often associated with CDW or other types of phase transitions. As mentioned above, a complicating factor is that the system may be inhomogeneous and involve a phase mixture, and it is important to recognize this in data analysis. Early studies of this system have yielded results that are mutually inconsistent, causing much confusion and speculations. However, more recent data from different groups are converging, and therefore sample reproducibility is no longer an issue.

We will show that a model involving the usual band structure and electron–phonon coupling can satisfactorily explain the photoemission results, provided that the presence of
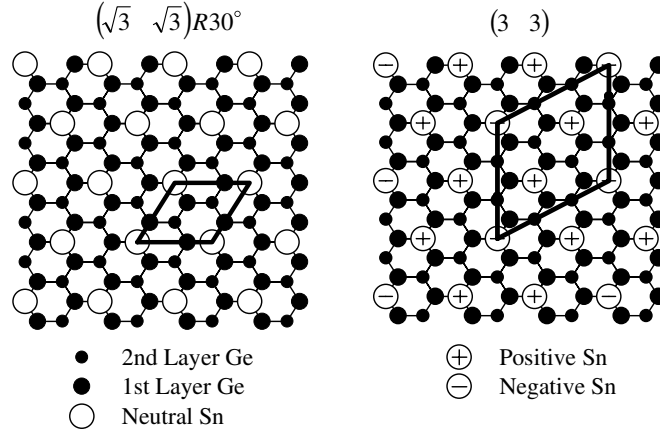
Figure 1. Schematic structural models for the $(\sqrt{3} \times \sqrt{3})$R30° and (3×3) phases of 1/3 ML of Sn on Ge(111). Sn atoms with positive and negative excess charges are labelled with a plus $(+)$ and a minus $(-)$ sign, respectively. The unit cells are shown.

the Ge defects, the resulting phase mixture, a narrow bandwidth near the Fermi level, and finite-temperature effects are taken into account [8]. This model has the appeal of simplicity, and is based on familiar ideas. There is no need to invoke dynamic effects or exotic many-body interactions, although these could still be important and may have ramifications in some other ways. These possibilities will be discussed. Other experimental results including those from core-level photoemission, photoelectron diffraction, and x-ray diffraction are reviewed, as the information is relevant to the static and dynamic structure of the system.

2. The problem

STM reveals that the surface is mostly $(\sqrt{3} \times \sqrt{3})$R30° reconstructed at room temperature. However, near the Ge defects, locally (3×3)-like patches can be found. These (3×3) areas grow as the sample temperature is lowered [1–4, 6]. Ignoring these defects for now, the $(\sqrt{3} \times \sqrt{3})$R30° reconstruction at room temperature is believed to involve Sn atoms adsorbed in threefold T_4 sites on a bulk-truncated Si(111) surface. A model of the atomic structure is shown in figure 1. Each $(\sqrt{3} \times \sqrt{3})$R30° unit cell contains one Sn adatom, and all Sn adatoms are equivalent. Although essentially all available experimental results support this T_4 model, there is a notable exception. A recent x-ray standing-wave analysis based on geometrical triangulation has indicated that the results are simply incompatible with the T_4 model [9]. Rather, the Sn atoms appear to be located in T_1 sites that are directly above the top-layer Ge atoms. This structure would seem extremely unlikely on the basis of either chemical intuition or total-energy consideration, but the issue has not been resolved yet. We will assume in this paper that the T_4 model stands. The threefold bonding for each Sn atom leaves an electron in a dangling bond, giving rise to a half-filled surface band. Figure 2 shows the results of a recent density functional band-structure calculation based on the local density approximation (LDA) [10]. The band has its maximum energy near the zone centre and disperses downward toward the zone boundary. The bandwidth is fairly narrow, suggesting that electron correlation may be important. A Van Hove singularity at M lies fairly close to the Fermi level, which constrains the group velocity nearby to a relatively low value.
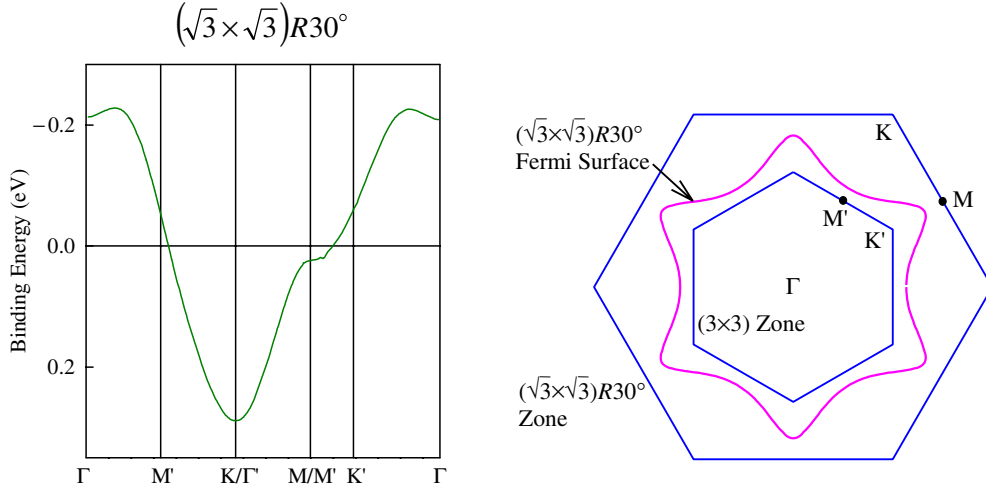
Figure 2. Calculated band structures of the $(\sqrt{3} \times \sqrt{3})$R30° phase and the Fermi surface. The two hexagons represent the $(\sqrt{3} \times \sqrt{3})$R30° and (3×3) BZ boundaries, and the high-symmetry points are labelled.

At low temperatures, the surface becomes (3×3). Figure 1 shows the atomic structure based on STM and other experimental evidence [1–6]. The unit cell becomes three times as large, and each unit cell now contains three Sn atoms. Two of them move downward and acquire a positive charge (labelled by a plus sign), and one moves upward and acquires a negative charge (labelled by a minus sign). The charge transfer results in a CDW, and the surface becomes corrugated. The charge transfer from the original, nominally neutral Sn adatoms creates contrast in STM images depending on the bias polarity. We shall refer to this transition as a CDW transition simply because of the charge transfer, although this is not necessarily a universal definition.

Also shown in figure 2 are the first Brillouin zones (BZ) for the $(\sqrt{3} \times \sqrt{3})$R30° and (3×3) surfaces and the calculated Fermi surface of the $(\sqrt{3} \times \sqrt{3})$R30° phase based on the LDA. In keeping with the usual language, we use the term Fermi surface, even though it is really a Fermi contour. The Fermi surface is hole-like, meaning that the states within are unoccupied. The Fermi surface does not contact the (3×3) BZ boundary, although it comes close along the sides of the hexagon. If the Fermi surface actually contacted the (3×3) BZ, such nesting could result in a (3×3) lattice distortion via electron–phonon coupling as in a Peierls transition. Without Fermi surface nesting and its associated lowering in electronic energy, it is unclear why the surface would make a transition into a (3×3) configuration.

This question has prompted many proposals for alternative interpretations. An early model involves a rehybridization mechanism [11]. The assumption is that the surface bandwidth is large enough to overlap the bulk band structure in the Ge substrate. Hybridization of the surface band with the bulk bands allows charge transfer and thus the Fermi surface becomes adjustable and can be made to mesh with the (3×3) BZ. Another model invoked strong electron correlation as the mechanism [12]. In an angle-resolved photoemission study, a dispersive peak in the normal phase was observed to transform into a nondispersive peak in the CDW phase accompanied by a depletion of the density of states near the Fermi level. The results were attributed to a metal–insulator transition caused by strong electron correlation. However, we now know that the bands remain dispersive in the low-temperature phase, and thus the basic

premise of this model appears to be unfounded. Yet another model suggests that the phase transition is an order–disorder transition [13]. The motivation for this model is the observed complexity of the photoemission spectra of the $(\sqrt{3} \times \sqrt{3})$R30° phase. There are more peaks than can be explained by the band structure shown in figure 2. Furthermore, results from the $(\sqrt{3} \times \sqrt{3})$R30° and (3×3) phases are fairly similar. Thus, the argument goes that the $(\sqrt{3} \times \sqrt{3})$R30° phase is just a disordered phase of (3×3). That is, the spectra should look similar, except for some disorder-induced broadening in the high-temperature phase. A closely related model, which has received much attention, is the dynamic fluctuation model [14–17]. The idea is similar, except that the disorder specifically involves time fluctuation. That is, the $(\sqrt{3} \times \sqrt{3})$R30° phase at any given moment is actually (3×3), but due to rapid fluctuation and time averaging, STM viewing of the surface gives the impression of a $(\sqrt{3} \times \sqrt{3})$R30° reconstruction with all Sn atoms apparently the same. Photoemission, on the other hand, is a rapid process and probes the instantaneous structure. The results should reflect the underlying (3×3) structure, but the spectral features might be broadened by the fluctuation. Yet other possibilities exist, including magnetic ground states, as suggested by theoretical many-body calculations [10, 18]. These calculations are not fully self-consistent or *ab initio*, and therefore it is hard to say for sure that the predictions can be compared with the experiment.

Related to the debate regarding the mechanism for the phase transition is the question of whether the (3×3) surface is metallic, semiconducting, or insulating with a correlation gap. Our own photoemission data, to be discussed below, agree well with the more recent data from other groups. The analysis and interpretation are, however, very different. The main idea is based on a Peierls transition involving pseudo-Fermi-surface nesting caused by defect doping.

3. Angle-resolved photoemission

Our photoemission measurements were performed at the Synchrotron Radiation Center in Stoughton, Wisconsin. All spectra shown were taken with a photon energy of 10 eV. Figure 3 shows a comparison between spectra taken at 80 and 300 K at several points in k-space. The bottom set of spectra, taken at normal emission (the Γ point in k-space), are nearly identical for the two phases. The other three sets of spectra were taken with polar emission angles of 17°, 22°, and 26° along the Γ–K′–M azimuth (see figure 2), and correspond to K′, midway between K′ and M′, and M′ on the (3×3) BZ boundary, respectively. The results are representative of what happens around the (3×3) BZ boundary—a broad peak with a somewhat strange lineshape near the Fermi level at room temperature is replaced by a sharper peak at 80 K, and simultaneously a well developed Fermi edge is replaced by an apparent gap at 80 K. This apparent gap opening was the motivation for the model based on strong electron correlation mentioned earlier [12].

The set of spectra in figure 3 might give the impression that the peaks are dispersionless. A more extensive set shows that this is not the case. A full set of spectra, taken along the Γ–M and Γ–K azimuths at 1° polar angle increments starting from the bottom spectra at normal emission, is shown in figure 4. The peaks are clearly dispersive, suggesting that a band-structure description is valid, and the system does not look like a Mott insulator. It just so happens that near the (3×3) BZ boundary, the peaks appear to be stationary partly due to a low dispersion.

The additional data along Γ–M again show that the leading peak at 300 K is much wider than that at 80 K, and the lineshape suggests that the peak is likely composed of unresolved components. The data along the Γ–K azimuth at 80 K show three dispersive peaks. The two near the Fermi level are derived from the Sn dangling bonds, and one of them appears to cross the Fermi level, in agreement with [13]. About midway between M′ and K, the valley between the
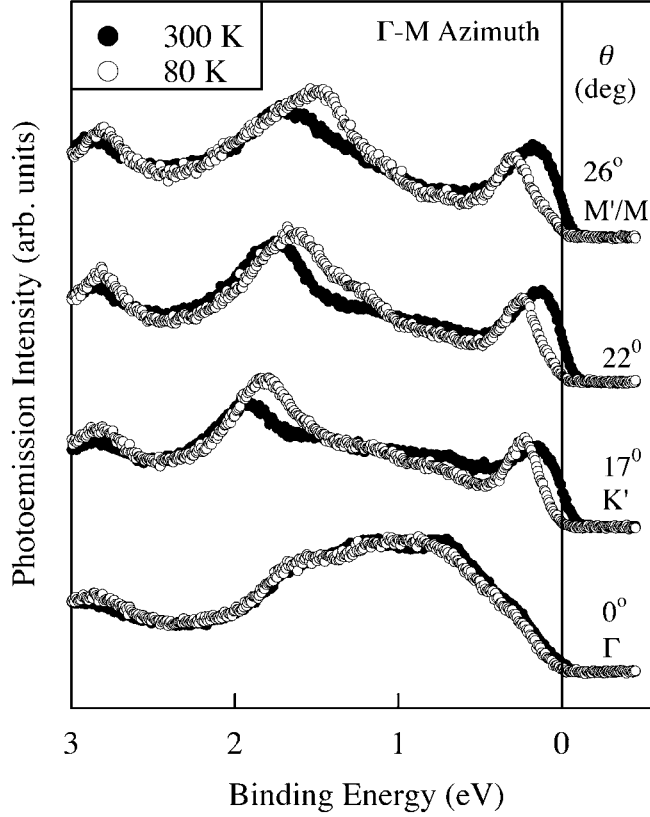
Figure 3. Comparison of photoemission spectra taken at 80 and 300 K for polar emission angles of 0°, 17°, 22°, and 26° along the Γ–M azimuth. They correspond to Γ, K′ midway between K′ and M′/M, and M′/M in the BZ.

two peaks at 80 K becomes filled in to form a broad feature at 300 K. A careful analysis shows that this lineshape cannot be accounted for by broadening of the 80 K spectra. Rather, the results can be well represented by the addition of a new peak located between the two original peaks.

On the basis of the band structure for the $(\sqrt{3} \times \sqrt{3})$R30° phase shown in figure 2, one would expect there to be no photoemission peak for small polar emission angles at room temperature because the band is above the Fermi level and unoccupied near the zone centre. As the polar emission angle increases, the photoelectron momentum in the surface plane increases correspondingly, and a single peak should appear beyond the Fermi wave vector and disperse toward higher binding energies. The experimental finding differs from the prediction in that up to three peaks appear. There are at least two possible interpretations for the multiple peaks. Our own interpretation is that the surface at 300 K is actually a mixture of the $(\sqrt{3} \times \sqrt{3})$R30° and the (3×3) phases due to defect pinning according to STM observations [8]. A single peak is expected for the pure $(\sqrt{3} \times \sqrt{3})$R30° phase, which should split into two for the (3×3) phase. Thus, a total of three peaks can be expected for the mixed phase at 300 K. At 80 K, the system is in the (3×3) phase. The intensity of the $(\sqrt{3} \times \sqrt{3})$R30° peak vanishes, and the spectra become simpler as seen in the experiment. An alternative interpretation, based on the dynamic fluctuation model or order–disorder transition, is that the 300 K spectra are just a broadened version of the corresponding 80 K spectra, because the surfaces are essentially the
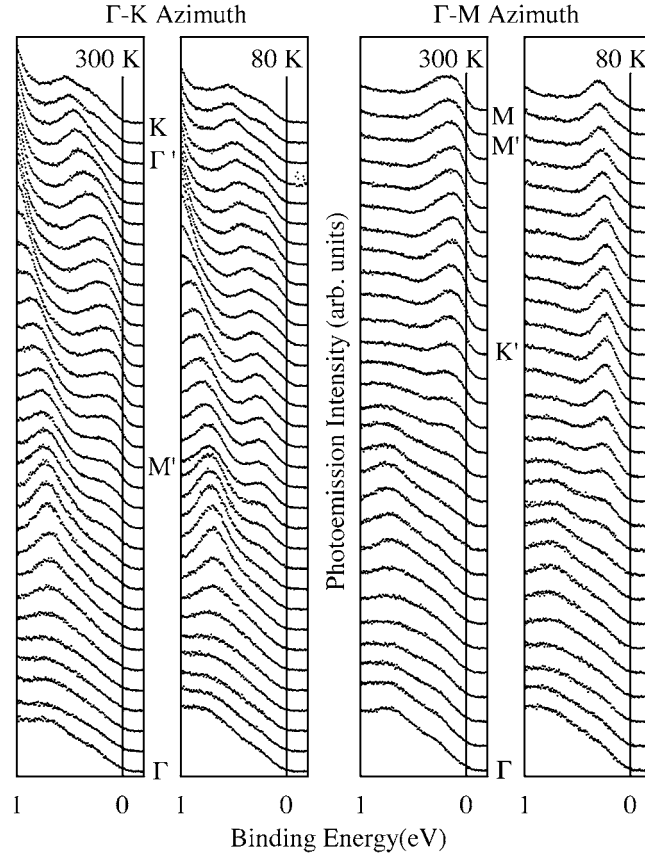
Figure 4. Photoemission spectra taken at 80 and 300 K along the Γ–K and Γ–M azimuths. In each set, the spectra are taken with a 1° increment in polar angle starting from the bottom spectrum taken at normal emission. The approximate locations in *k*-space are indicated for features near the Fermi level.

same as far as photoemission is concerned [13, 14]. However, as mentioned above, a detailed fit of the data shows that a simple broadening does not quite explain the differences between the 300 and 80 K data.

To further develop our mixed-phase interpretation, we show in figure 5 difference spectra along the two azimuths obtained by subtracting the 80 K data from the 300 K data, with each pair of spectra normalized to the same integrated intensity between 0 and 4 eV binding energy. The phase transition causes a transfer of spectral weight among the different peaks. As expected, the main feature of the difference spectra along each direction is a prominent peak near the Fermi level. This should correspond to the $(\sqrt{3} \times \sqrt{3})$R30° peak based on the band structure shown in figure 2. Some weak negative features are also expected and observed in the difference spectra because of the overall normalization, spectral weight transfer, over-subtraction at the (3×3) peak positions, and possibly background effects. These negative features are ignored in our analysis. The solid curves through the data points are best fits assuming a Lorentzian peak with constant width multiplied by the Fermi–Dirac function. A constant peak width is compatible with the notion that the width is dominated by defect scattering. While the peak is below the Fermi level, its intensity remains fairly constant from
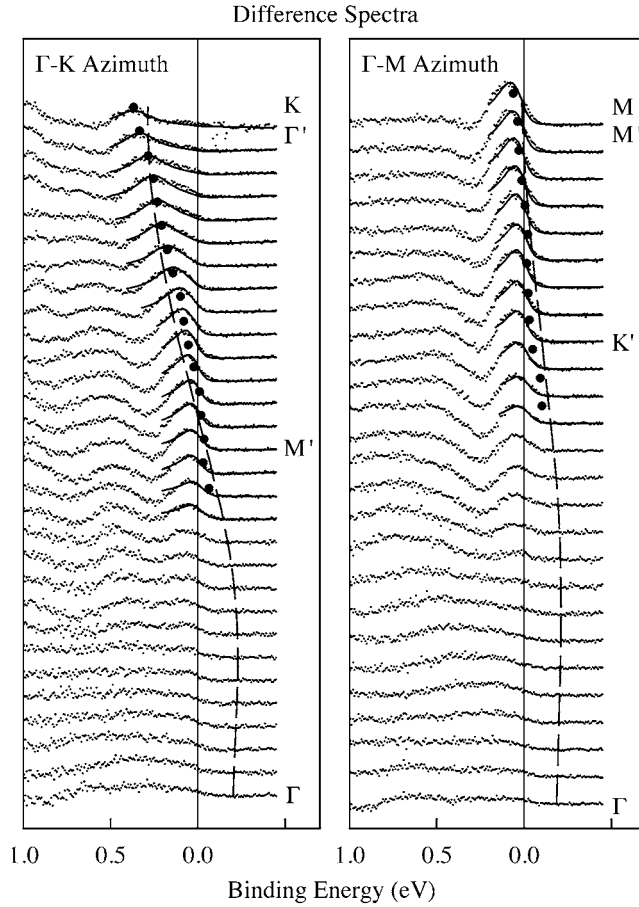
Figure 5. Difference spectra along the Γ–K and Γ–M azimuths obtained by subtracting the 80 K spectra from the 300 K spectra. The curves through the data points are best fits, and the dashed curves are dispersion curves based on a band-structure calculation.

the fit. Thus, it is reasonable to extend the analysis over a limited range as the peak moves above the Fermi level, leaving only a tail in the spectra. The peak positions deduced from the fit are shown as circles in figure 5, and the peak intensities vary by less than 10% near and above the Fermi level. The dashed curves indicate the expected peak dispersions for the pure $(\sqrt{3} \times \sqrt{3})R30°$ phase based on the LDA calculation shown in figure 2. They are in good agreement with the experiment. This good agreement is strong evidence supporting the mixed-phase interpretation.

An alternative approach of analysis is to fit the original spectra with a set of peaks. However, the peaks in figure 4 are not well resolved, and numerous assumptions must be made with many fitting parameters. This is less convincing, in our opinion. Taking the difference spectra, by contrast, is a straightforward procedure with few assumptions. If the dynamic fluctuation model were correct, which argues that the two sets of spectra at low temperature and room temperature are essentially the same except for peak broadening, the difference spectra would not yield a single dominant peak. Instead, there would be weak negative features at the peak positions surrounded by slightly positive wings or background.
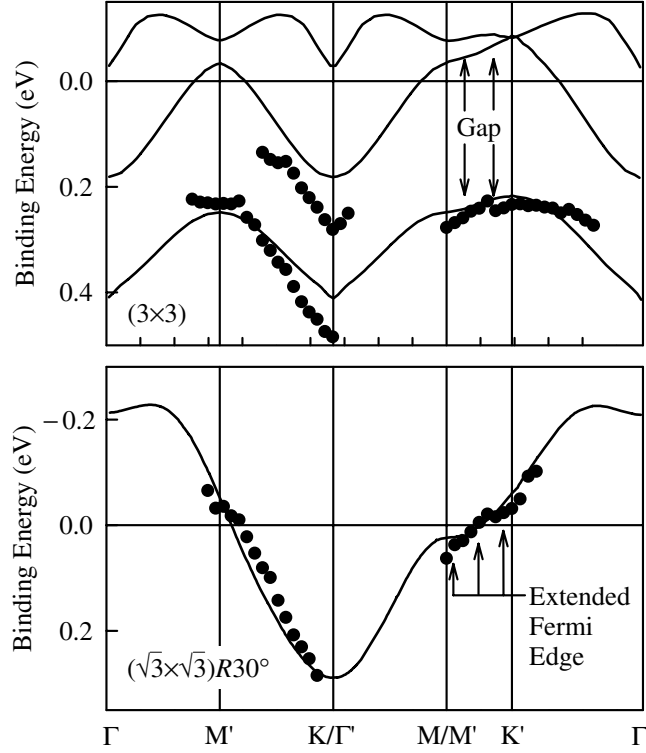
Figure 6. Theoretical band dispersions (curves) and experimental results (circles) for the (3 × 3) phase (upper panel) and the ($\sqrt{3} \times \sqrt{3}$)R30° phase (lower panel).

The lower panel of figure 6 shows the band dispersion derived from the peaks in the difference spectra (circles) and the LDA band (curve). Again, the agreement is quite good, lending strong support to our interpretation. As noted above, the Fermi surface does not mesh with the (3 × 3) BZ, yet the 300 K spectra in figure 4 indicate a Fermi edge all around the (3 × 3) zone boundary. This region of 'extended Fermi edge' is indicated in the lower panel of figure 6. In this region, the band dispersion lies within just several tens of meV from the Fermi level due to a relatively low group velocity. This low dispersion, the finite peak width (probably dominated by defect scattering), and thermal broadening ($k_B T = 26$ meV at room temperature) conspire to give rise to the extended Fermi edge.

The circles in the upper panel of figure 6 show the measured band dispersions for the (3 × 3) phase. The solid curves are theoretical results from an LDA calculation with electron correlation (on-site Coulomb interaction) included within a generalized Hubbard model [19–21]. The agreement between experiment and this LDA Hubbard calculation is quite good. Between M′ and Γ′, the single band for the ($\sqrt{3} \times \sqrt{3}$)R30° phase (lower panel) is split into three bands in the (3 × 3) phase. The lower two bands are observed by means of photoemission, while the highest band is unoccupied and therefore not observed. Between M′ and K′, the ($\sqrt{3} \times \sqrt{3}$)R30° band also splits into three bands in the (3 × 3) phase. Only the lowest band is occupied, and its energy is much lower than the corresponding ($\sqrt{3} \times \sqrt{3}$)R30° band near the Fermi level. This energy shift accounts for the apparent gap opening in the spectra around the (3 × 3) BZ boundary, as marked in figure 6. Despite the band splitting and apparent gap over a portion of the BZ, the (3 × 3) surface remains metallic [17].
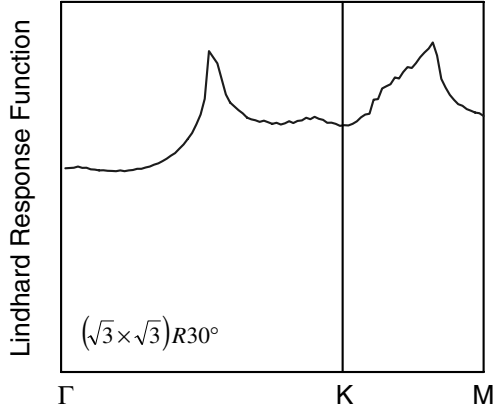
Figure 7. The calculated Lindhard response function for the ideal $(\sqrt{3} \times \sqrt{3})R30°$ phase along high-symmetry directions in the BZ.

4. Mechanism for the (3 × 3) response

With the photoemission results and band structure satisfactorily explained, we now turn to the question of why the surface undergoes a (3 × 3) phase transition. The same LDA Hubbard calculation [21] shows that the $(\sqrt{3} \times \sqrt{3})R30°$ and (3 × 3) phases have nearly the same energy, with a difference of just a few meV per Sn atom. This difference is about at the limit of accuracy of the calculation, and it is difficult to tell which reconstruction actually has the lower energy. Despite the extended Fermi edge as observed in the experiment, there is not an exact nesting of the Fermi surface. Thus any electronic energy lowering caused by the lattice distortion must be small, and this is in agreement with the LDA Hubbard calculation.

A standard test for a mechanism based on electron–phonon coupling is to compute the response function. If the response function peaks strongly at a commensurate point in k-space, the corresponding lattice distortion would be a likely candidate for a phase transition. The Lindhard response function is given by

$$\chi(q) = \int_{BZ} \frac{dk}{(2\pi)^2} \frac{n_k - n_{k+q}}{E_{k+q} - E_k} \tag{1}$$

where n denotes the state occupation. Figure 7 shows the calculated χ for the $(\sqrt{3} \times \sqrt{3})R30°$ phase [10]. The calculation employs the band structure shown in figures 2 and 6, which have been verified by our photoemission results. Thermal smearing effects have been ignored for simplicity, and thus this is effectively a $T = 0$ calculation. This plot covers the most important high-symmetry directions. The K points in the $(\sqrt{3} \times \sqrt{3})R30°$ BZ correspond to zone centres for the (3 × 3) reconstruction. A large peak at K would be an indication of a tendency for the system to undergo a (3 × 3) Peierls distortion. The plot in figure 7 shows two peaks, but none is at the K point.

The left panel of figure 8 is a two-dimensional plot of the response function using a greyscale representation. This is to make certain that we do not miss any other strong peaks in k-space. The dashed hexagon represents the first BZ of the $(\sqrt{3} \times \sqrt{3})R30°$ phase, and the corners are the K points. Again, high intensities at K points would indicate a strong (3 × 3) response, but this is not the case. The pattern is rather diffuse, indicating poor or no nesting.

The fact that defects can induce the (3 × 3) phase transition locally at room temperature as observed by STM [1–4, 6] is an important clue. The defects, being electron donors according to STM studies, can cause an upward shift of the local Fermi level. Shown in the middle and right panels of figure 8 are calculated response functions with the Fermi level shifted upward by $\Delta E_F = 25$ and 50 meV, respectively. These are not very large shifts (compared to
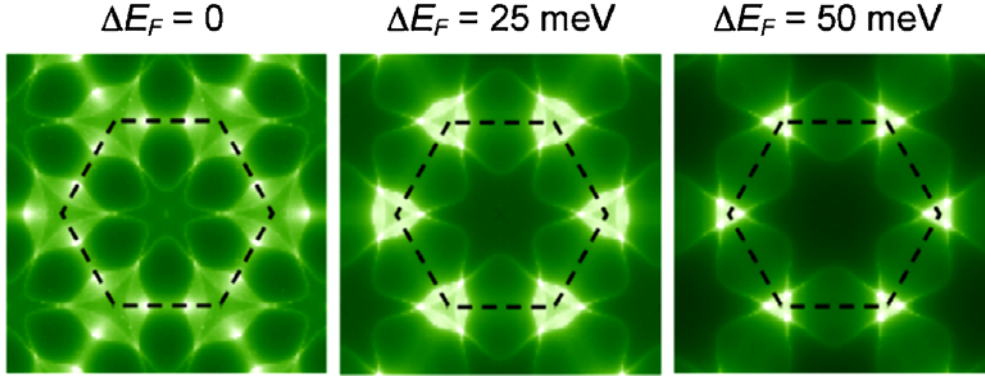
Figure 8. Greyscale maps showing the calculated Lindhard response functions for the ideal $(\sqrt{3} \times \sqrt{3})$R30° phase (left panel) and the same with the Fermi level shifted upward by 25 meV (middle panel) and 50 meV (right panel) relative to the band. The dashed hexagons indicate the $(\sqrt{3} \times \sqrt{3})$R30° BZ. The calculation assumes $T = 0$ K.
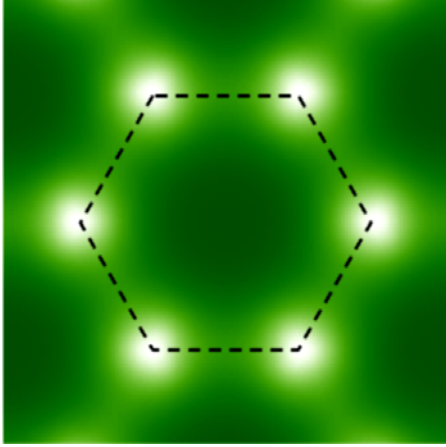

Figure 9. Greyscale maps showing the calculated Lindhard response functions for the ideal $(\sqrt{3} \times \sqrt{3})$R30° phase at $T = 300$ K with the Fermi level shifted upward by 50 meV.

$k_B T = 26$ meV at room temperature), and yet the change in the response function is substantial. As ΔE_F increases, there is a rapid concentration of intensity near the K points, indicating a (3×3) response. This high sensitivity of the response function to a shift in Fermi level is a consequence of the low band dispersion along M/M′–K′ as seen in the lower panel of figure 6. This is also responsible for the extended Fermi edge discussed above.

To assess the thermal smearing effects ignored so far, figure 9 shows the response function for $\Delta E_F = 50$ meV calculated with the thermal population factor taken into account at $T = 300$ K. As expected, the pattern is smoothed out, and the only features left are six fuzzy intensity maxima centred on the K points. The fuzziness, or the width of each intensity maximum, is related to the expected defect-induced (3×3) domain size in real space through the uncertainty principle. From the results in figure 9, one can estimate that the domain size is about a few atomic spacings, which is roughly what STM shows at room temperature.

The above discussion suggests that the basic mechanism for the phase transition is the same as in traditional Peierls CDW materials. That is, electron–phonon coupling with pseudo-
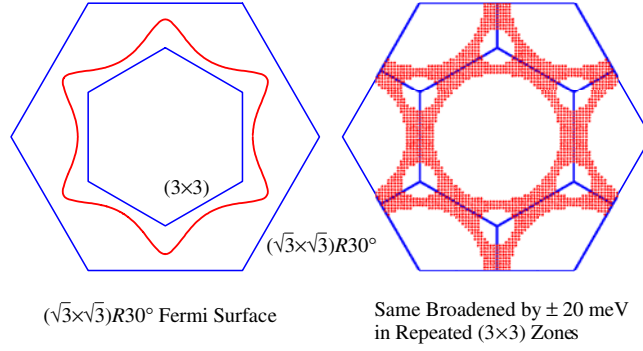
(3×3)

($\sqrt{3} \times \sqrt{3}$)$R30°$

($\sqrt{3} \times \sqrt{3}$)$R30°$ Fermi Surface

Same Broadened by ± 20 meV
in Repeated (3×3) Zones

Figure 10. The left panel shows the calculated Fermi surface for the ideal ($\sqrt{3} \times \sqrt{3}$)$R30°$ phase relative to the ($\sqrt{3} \times \sqrt{3}$)$R30°$ BZ (large hexagon) and the (3 × 3) BZ (small hexagon). The right panel shows the same Fermi surface broadened by ±20 meV and folded according to the (3 × 3) symmetry. The resulting broadened Fermi surface meshes well with the (3 × 3) BZ boundary.

Fermi-surface nesting caused by defect doping is the source of the lattice instability. This type of instability is usually described in terms of phonon softening. That is, a phonon near the zone boundary has a temperature-dependent frequency. The frequency lowers for decreasing temperatures and becomes zero at the transition temperature. Below the transition temperature, a static lattice distortion sets in and grows as the temperature decreases further. This soft-mode behaviour has been verified by a recent density functional calculation of the phonon dispersion curves of this system [22]. The actual behaviour of the system is somewhat more complicated due to the defects. Instead of a simple, homogeneous phase transition over the entire surface, STM shows, as the temperature is lowered, that the (3 × 3) regions pinned by the defects grow and eventually overlap to form a fully developed (3 × 3) phase at low temperatures.

The concept of pseudo-Fermi-surface nesting is further illustrated in figure 10. Here, the perfectly sharp Fermi surface on the left for the ideal ($\sqrt{3} \times \sqrt{3}$)$R30°$ surface is broadened by ±20 meV and folded according to the (3 × 3) symmetry. The resulting 'broadened Fermi surface' shown on the right matches pretty well the (3 × 3) BZ boundaries. This is related to the observed extended Fermi edge mentioned above. It is important to recognize that a small bandwidth (and a small group velocity) can make a system quite sensitive to doping and thermal effects. Many-body effects also tend to be more important in the case of a small bandwidth. However, the behaviour of the Sn/Ge system can be well explained without resorting to complicated many-body effects.

5. Real-space response based on a tight-binding calculation

A simple extension of the same model and ideas allows us to evaluate the real-space response of the system to a charged impurity. The results should be directly comparable to STM observations of the charge distribution around a Ge defect, and this can be taken as an additional test of the model. The starting point is a tight-binding model fit to the band structure shown in figure 2 with two-body interactions extending to the sixth neighbours [10]. Our calculation employs a two-dimensional $N \times N$ cluster of Sn atoms arranged in a hexagonal net. The potential energy for the central atom is shifted slightly by $\Delta V = +0.001$ eV to create an electron deficiency, thus simulating the effect of a defect as an electron donor. The potential energy shift adopted here is very small, because we wish to keep the system in the linear response regime. The tight-binding Hamiltonian, with the impurity potential added, is diagonalized
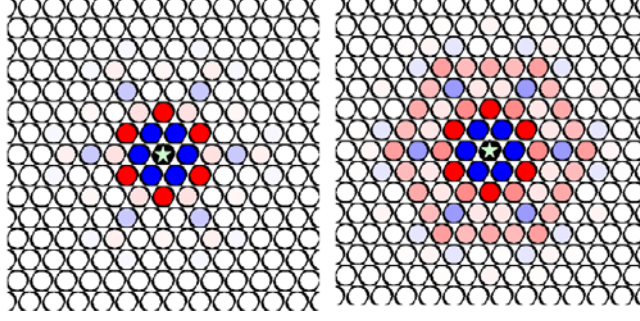
Figure 11. Left panel: calculated charge response to a donor impurity at the centre of a 41×41 cluster within a tight-binding model. The central impurity atom is marked by a star. Red (blue) is used to indicate a positive (negative) charge, and neutral atoms are shown in white. The intensity of the red or blue is an indication of the amount of excess charge. Right panel: the same except that the excess positive and negative charges have been converted by a square-root function to compress the intensity scale in order to show details.

to yield eigenvectors and eigenvalues. The resulting charge redistribution on the lattice is calculated according to

$$Q_{m,n} = -e \left[\sum_i \frac{\left| \psi_{m,n}^i \right|^2}{1 + \exp\left(E^i / k_B T \right)} - 1 \right] \qquad (2)$$

where e is the electronic charge, m and n are site indices (each between 1 and N), i is the state index (between 1 and $2N^2$, where the factor of 2 comes from electron spin), E is the state energy (with the Fermi level at zero), and ψ is the normalized eigenvector. The absolute square of the eigenvector yields the probability, and the denominator in equation (2) comes from the Fermi–Dirac distribution function. A positive (negative) Q corresponds to depletion (accumulation) of electronic charge.

The results for $N = 41$ and $T = 300$ K are shown in the left panel of figure 11, which covers only a portion of the lattice near the central impurity atom. Each circle represents an atom, and a star marks the central atom. Red (blue) is used to indicate a positive (negative) charge, and neutral atoms are shown in white. The intensity of the red or blue is an indication of the amount of the excess charge. The response to the impurity is fairly local, and we have verified that the cluster is large enough to avoid boundary effects. The spatial range of the response increases at lower temperatures to a fairly long range (results not shown). This is in qualitative agreement with STM observations that the effective range of the Ge defect increases at low temperatures.

The main features of the charge response include six blue atoms in the first shell surrounding the central atom and six red atoms in the next shell. Beyond that, the charge response decays rapidly. The results look very similar to what STM shows at room temperature; namely, the local response is (3×3). Referring back to the atomic structure model in figure 1, the negative atoms form a hexagonal net, while the positive atoms, twice as many, form a honeycomb pattern. The honeycomb pattern consists of hexagonal rings, each surrounding a negative atom. In figure 11, the blue atoms in the first shell form a hexagonal ring. This is the basic unit of a (3×3) reconstruction. Compared with the ideal pure (3×3) phase, the phase of the CDW is reversed. That is, instead of a red hexagonal ring, we have here a blue hexagonal ring surrounding an impurity atom. This phase reversal has been discussed at length in the literature, and is sometimes observed in certain domains at low temperatures [6].

One wonders, since the phase is reversed right next to the defect, how the phase can become correct at low temperatures when large (3×3) domains are formed. An explanation offered was that defect–defect interaction at low temperatures results in an interference pattern that exhibits the correct (3×3) phase. This effect is enhanced by a subtle transition at low temperatures whereby the positions of Ge defects become spatially correlated. At intermediate temperatures, the surface structure is rather complicated, as one can imagine. A detailed analysis of the surface pattern based on STM can be found in the literature [6].

In the present calculation, we wish to examine the phase of the charge oscillations at larger distances (Friedel oscillations). These oscillations die away very quickly, and in order to see the effect more clearly, we present in the right panel of figure 11 the signed square root of the charge, $\mathrm{sgn}(Q)\sqrt{|Q|}$, with a constant background subtracted. The square-root function compresses the intensity scale, and thus weak features become more visible. One can see that the six first neighbours to the central impurity atom forming a blue hexagon, when amplified three times, map onto another six blue atoms. Each of these blue atoms is surrounded by six pink atoms forming a hexagonal ring. Each of these blue atoms is also accompanied by two other blue atoms further out to form a hexagonal net configuration. Thus, locally, we have a (3×3) configuration with the correct phase.

The tight-binding model shows that the real-space response is characterized by a (3×3) configuration in agreement with the reciprocal-space argument in terms of a response function. This is not surprising because both are quantum mechanical calculations based on a linear response of the system with the same starting band structure. One question is whether or not we can carry the model further. For example, in the tight-binding model, one might be tempted to increase the impurity potential to something more representative of the real system. This is easy to do, and one can also incorporate randomly distributed or correlated impurities in the model. We have tried these ideas at various temperatures and the results are complex and not particularly illuminating. One problem is that the system response is necessarily nonlinear. The band structure changes as the system distorts, and this change is not in the present model. Linear response theories allow us to determine the initial trend, but not the detailed system evolution at later stages. What we have achieved here is to demonstrate the initial trend of the system toward forming a (3×3) configuration with defect doping.

6. Discussion

6.1. Dynamic effects

Our model is successful thus far in explaining the results from angle-resolved photoemission and the essential physics of the system. With simplicity in mind, we have not worried too much about the dynamic behaviour, or possible time fluctuation of the system. Of course, all systems exhibit lattice vibrations. These vibrations, or phonons, can give rise to a temperature-dependent spectral broadening, as has been observed in numerous systems. In our model, we have assumed that these dynamic effects are just minor details with no major consequences. The dynamic fluctuation model, on the other hand, assumes that lattice fluctuation is the key feature. This concept has received considerable attention, and it is useful to address this issue in some detail. In reading through the literature, it is actually unclear exactly what dynamic fluctuation means in some cases. Some authors seem to take lattice vibrations, or the usual phonons, as a form of dynamic fluctuation. This is not our preference, as there is no reason to introduce new terminology for an old concept. At some level, the ongoing controversy seems to be partly a matter of semantics.

Assuming that the dynamic fluctuation model is correct, namely, the system at any instant is in a (3 × 3) geometry at room temperature, the motion of each Sn atom cannot be a simple up–down harmonic motion. Rather, it is probably more like quantum tunnelling between two positions. One of the two positions is up, with the atom negatively charged, and the other is down, with the atom positively charged. The probability for the atom to be in the down position must be twice as large as that for the up position in order to yield a statistically uniform appearance for the three atoms in a unit cell as observed by STM. Furthermore, the motions of neighbouring Sn atoms are correlated such that at a given instant, the (3 × 3) configuration is preserved. When an up atom changes into a down atom, the phase of the (3 × 3) wave shifts. To accomplish this correlated motion, one possible scenario is a sliding CDW [23]. That is, a CDW travels within the plane of the surface, and thus the (3 × 3) phase for each Sn atom varies periodically and averages to zero. Sliding charge-density waves are well known in traditional CDW materials, but mostly for incommensurate phases. Such motions are much harder for commensurate waves. Defect pinning of CDW is also a well known phenomenon. Usually, this is a temperature-dependent effect—namely, a CDW becomes depinned and moves above a certain temperature. The case of Ge/Si is different, however. The temperature dependence seems to be through the growth of statically pinned areas. To make the sliding CDW scenario work, one would need a description or explanation for the interaction of a sliding CDW with defects in this case, and, in particular, for boundary effects where a dynamically fluctuating domain meets a statically pinned area.

One interesting question is that of the frequency spectrum of the dynamic fluctuation. Is there a well defined frequency, such as in the case of a sliding CDW with a constant velocity? Or is this broad band? If there is a well defined frequency, perhaps it is possible to detect it through inelastic scattering by electrons, photons, or neutrons. As far as we know, no such measurements have been made. There may be other scenarios for dynamic fluctuation, such as the dynamic stripes in high-temperature superconductors, but we will not speculate any further. Our results can be explained without dynamic fluctuation.

6.2. Photoemission from the Sn core level

A key question in this debate is that of whether or not the Sn atoms occupy equivalent sites at room temperature. In the simplified picture of the $(\sqrt{3} \times \sqrt{3})R30°$ surface, all Sn atoms are equivalent (apart from the usual lattice vibrations). This is not so within the dynamic fluctuation model at any given moment in time. Core-level spectroscopy, which yields a statistical sampling of all instantaneous atomic configurations, would seem to be a good test. A true $(\sqrt{3} \times \sqrt{3})R30°$ lattice, with all equilibrium lattice sites being equivalent, would give rise to a single core-level component, which may be broadened by lattice vibrations. By contrast, a dynamically fluctuating (3 × 3) phase, with a time-averaged $(\sqrt{3} \times \sqrt{3})R30°$ structure, would give rise to two components due to the charge transfer or inequivalent atomic bonding geometries for the up and down atoms in the (3 × 3) phase. However, the problem is not clear-cut because the surface at room temperature is actually in a mixed phase due to defects and local pinning. A simple analysis based on STM estimates of the defect-pinned area reveals that the core-level lineshape can be fairly complicated even for a static lattice. The experimentally observed lineshapes are indeed complicated. Both the mixed-phase model [24] and the dynamic fluctuation model [17] have been used to explain the results with partial success.

Figure 12 shows core-level spectra taken at both room temperature and low temperature for a Sn coverage of 0.35 ML [17]. The lineshapes are complicated. Let us focus on the lineshape at low temperature first. There are two major peaks seen by inspection (C1 and C2), but
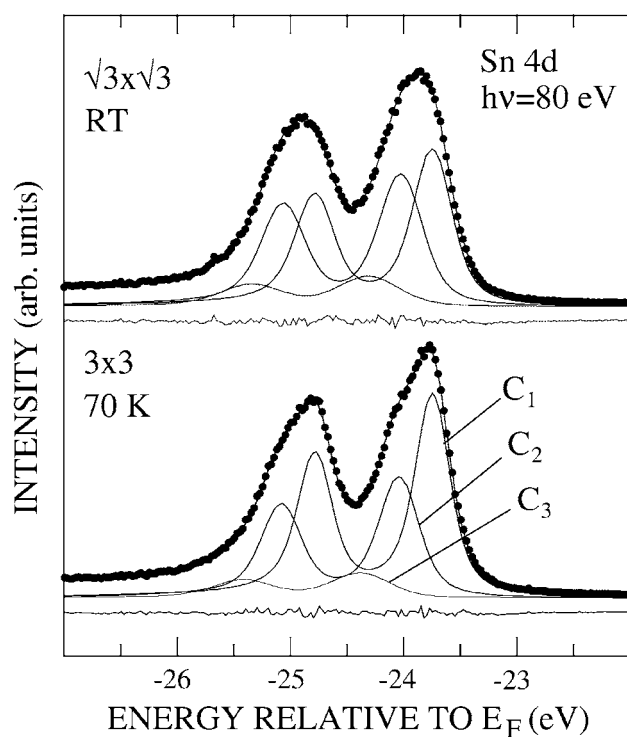
Figure 12. Sn 4d core-level spectra taken from the ($\sqrt{3} \times \sqrt{3}$)R30° and (3 × 3) surfaces for 0.35 ML Sn coverage (from [17]). The circles are data points and the curves are results of a fit. The components are labelled C1, C2, and C3, and the bottom curve represents the residue of the fit.

curve fitting suggests that there are definitely more peaks (C3). Since these peaks are not well resolved, a detailed quantitative analysis is difficult. One problem, though, is the intensity ratio between the two major peaks (C1 and C2) at low temperatures. Presumably the surface is in a fairly pure (3 × 3) phase, and two components corresponding to the positively and negatively charged Sn atoms are expected with an intensity ratio of 2 to 1. The component corresponding to the positively charged atoms should have a larger binding energy, because it would take more energy to remove an electron from a positively charged atom. The observed intensity ratio varies from experiment to experiment. This is partly due to uncertainties in coverage, and partly due to photoelectron diffraction effects. A photoelectron leaving the emitting atom reaches the detector via many possible paths, including scattering by nearby atoms. Interference can give rise to complicated intensity variations as a function of emission direction and energy. The physical situation is like a point emitter sitting on a three-dimensional diffraction grating (the substrate crystal lattice). Such diffraction effects must be carefully analysed in order to avoid large errors. Ideally, the intensity ratio should be evaluated using angle-integrated photoemission spectra averaged over a wide range of photon energy. In practice, this averaging is almost never carried out (fully).

The spectra in figure 12, taken with an angle-resolved geometry and with a carefully calibrated Sn coverage, show a C2:C1 intensity ratio of about 1:1.5 between the high- and low-binding-energy components at low temperatures. This is very different from the expected 2:1 ratio, and the difference seems to be well beyond the usual uncertainties arising from diffraction

effects. One explanation offered was that final-state screening effects are so different for the two types of atoms as to reverse the binding energy order [17]. Thus the more intense component, at a lower binding energy, actually corresponds to the positive (down) atoms. This would be an unusual situation because numerous core-level studies have established a correlation between charge transfer and core-level shifts, and few cases have been reported to have the binding energy shift reversed due to final-state screening. A calculation would be useful to verify this case.

The room temperature lineshape shown in figure 12 is very much smeared out, but it is clearly made up of multiple components. A three-component fit is shown, but there could be many more components. Defects are known to have a relatively long-range effect, and the broad lineshape is consistent with a mixed phase with multiple shifts at room temperature. Thermal broadening may be particularly strong in this case because of a partially softened phonon mode [22]. The broad lineshape is also consistent with the dynamic fluctuation model. By visual inspection, the room temperature spectrum may be interpreted as just a broadened version of the low-temperature spectrum [15, 17, 22].

The three-component analysis shown in figure 12 represents the simplest assumption that remains reasonable for a satisfactory fit. However, the spectra can surely be fitted with more components and, with uncertainties in peak assignments, it becomes extremely difficult to use the information as a basis for definitive statements. Core-level spectroscopy is a very powerful technique, but its utility is limited in cases with multiple unresolved components as in the present case. The experimental core-level lineshape of Sn/Ge is still being debated. No single model offers a completely satisfactory, quantitative, and definitive explanation for all details.

6.3. Many-body effects and magnetic ground states

As mentioned earlier, many-body effects could be important. A simple test is to compare the bandwidth with the lifetime broadening of the quasiparticle. If the bandwidth is small in comparison, the band picture loses its significance, because the quasiparticle does not live long enough to be described in terms of wave propagation in a periodic potential. An equivalent argument is that the particle has such a short mean free path that it is effectively localized on one site. Our photoemission results clearly show band dispersion. It is relatively small, but not too small compared with the peak width, and thus band structure should remain a pretty good description. The (3×3) case is a little worse, because the bandwidth becomes smaller after band splitting. Another issue is the possibility of a magnetic ground state as suggested by many-body calculations with suitable choices of parameters [10]. A magnetic ground state is possible when the spin degrees of freedom are coupled to the orbital or lattice degrees of freedom in the calculation. Yet other possibilities exist [18]. Since available calculations are not based on first-principles or *ab initio* methods, it is difficult to assess the importance of these many-body effects. The good agreement between theory and experiment as discussed above in our analysis would suggest that the phase transition does not involve complicated electron correlation effects such as correlation-induced metal–insulator transitions. Can one detect magnetic effects in a surface layer? Theoretically, it is possible, but in practice, it is a tough experiment.

6.4. Diffraction determination of structure

X-ray diffraction is usually the method of choice for structural determination. The method is robust with few uncertainties for bulk single crystals, but this is not necessarily so for surfaces.

Because of the possibility of multilayer relaxation to a large depth and layer-dependent Debye–Waller factors, the analysis can involve a large number of parameters. X-ray diffraction has been applied to Sn/Ge by several groups [5, 16, 25], but the results remain controversial. Recent studies have yielded completely different conclusions. In two cases, the conclusion is that the simple model without dynamic fluctuation represents the correct structure [5, 25]. In another study [16], the dynamic fluctuation model is shown to be the correct model. In other words, the surface is corrugated at both room temperature and low temperature. In this latter analysis involving a fairly large data set, horizontal and vertical atomic displacements up to the third bilayer of the substrate are allowed in the structural optimization, and the total number of independent structural parameters is 30. The χ^2-value is 1.48 for the best fit for the (3×3) phase and 1.96 for a fit to the $(\sqrt{3} \times \sqrt{3})\mathrm{R}30°$ phase assuming a flat Sn layer with no corrugation (but with a Debye–Waller factor to account for lattice vibrations). The best fit for (3×3), however, yields a structure involving two Sn atoms moved up and one Sn atom moved down. This is opposite to what has been reported in the literature, namely, two atoms down and one atom up. Forcing the Sn atoms into this configuration in the x-ray analysis results in a larger value of χ^2 of 2.24.

A photoelectron diffraction analysis of the Sn core level has been performed for the (3×3) phase [26]. A two-component analysis assuming that the lower-binding-energy component corresponds to the positive Sn atoms results in a corrugated Sn layer with the negative atom in a unit cell moved up relative to the two positive atoms. This is opposite to the x-ray analysis result just mentioned. However, it is hard to say whether a two-component fit represents a good approximation in this case.

This is the current state of affairs, and the disagreements remain puzzling. Note that the diffraction spots from $(\sqrt{3} \times \sqrt{3})\mathrm{R}30°$ form a subset of the (3×3) spots. As the system temperature goes up, the distinct (3×3) spots become weaker and broader according to the same x-ray study. The spots actually persist to temperatures significantly higher than the transition temperature. This has been interpreted within the dynamic fluctuation model in terms of a (3×3) order that is becoming increasingly short ranged [16]. On the other hand, the persistence of a weak (3×3) diffraction pattern is also consistent with the presence of (3×3) patches pinned by defects at room temperature. Thus, the diffraction intensity variation can be equally well explained by the mixed-phase model without dynamic fluctuation. Up to now, diffraction studies have not provided the distinction needed to separate out the different models.

7. Summary and conclusions

1/3 ML of Sn on a Ge(111) surface is a seemingly simple adsorbate system, and yet it exhibits an interesting CDW phase transition with features that are characteristic of complex systems. A few percent of Ge defects in the Sn layer leads to a complex pattern of mixed phases over a wide temperature range. Angle-resolved photoemission results for the room temperature $(\sqrt{3} \times \sqrt{3})\mathrm{R}30°$ phase are complex, and can be best explained in terms of a linear combination of an uncorrugated $(\sqrt{3} \times \sqrt{3})\mathrm{R}30°$ phase and a corrugated (3×3) CDW phase. The band structure for the $(\sqrt{3} \times \sqrt{3})\mathrm{R}30°$ phase, extracted from difference spectra, is in excellent agreement with LDA calculations assuming an uncorrugated surface. The experimental band structure of the (3×3) phase is in good agreement with an LDA Hubbard calculation. A portion of the $(\sqrt{3} \times \sqrt{3})\mathrm{R}30°$ band lies very close to the Fermi level around the (3×3) BZ boundary. This, with broadening, leads to an extended Fermi edge in the photoemission spectra. The transition to (3×3) causes band splitting, thus suppressing emission near the Fermi level, but the system remains in a metallic state.

There is no Fermi-level nesting for the ideal $(\sqrt{3} \times \sqrt{3})R30°$ phase. However, defect doping can lead to a strong local (3×3) response according to a calculated response function. This sensitivity is due to a small overall bandwidth and a very small group velocity of the band near the Fermi level. Defect-induced pseudo-Fermi-surface nesting is believed to be the driving mechanism for the phase transition, which is in agreement with STM studies that show the central role played by defects. Nesting results in a lowering of the electronic energy, and electron–phonon coupling leads to phonon softening and eventually a static distortion as in the usual Peierls transitions. A similar linear response model involving a tight-binding cluster calculation using the same band structure is employed to evaluate the real-space charge response to a defect. The results are very similar to what STM reveals. The issue of phase reversal— namely, the spatial arrangement of the positively and negatively charged Sn adatoms—is clarified.

Is there a phase transition for a defect-free surface, assuming that such a surface can be prepared? We do not know. If there is one, it is likely that the transition temperature would be much lower. This would be an interesting experiment to try. Although we do not know for certain, the Ge defects on the surface, at a concentration of a few percent, appear to be intrinsic and may represent a quasi-equilibrium property of the system for the sample preparation temperature needed for annealing. Perhaps other routes for surface preparation involving lower temperatures can lead to a lower defect density, or maybe there are ways to increase the surface defect density. Such experiments would be helpful in establishing the connection between the CDW transition and the defect density. Surfaces prepared with Sn and other dopants might also offer useful information, but the added complexity can be a problem [27].

An alternative interpretation of the photoemission results is the dynamic fluctuation model, even though it is not quite consistent with the analysis based on difference spectra. This model assumes that the surface at room temperature remains corrugated in a (3×3) phase at any given instant. Fluctuation leads to time averaging and an impression of a $(\sqrt{3} \times \sqrt{3})R30°$ surface. Possible scenarios for such fluctuation are discussed. Core-level photoemission, x-ray diffraction, and photoelectron diffraction have been employed as a means for statistical sampling of the instantaneous structure of this system. However, the results are sometimes inconsistent and largely inconclusive, partly due to the intrinsic complexity of the system. Other explanations based on many-body effects have been proposed, but our photoemission results suggest that these are unlikely to play an important role in the CDW transition.

Acknowledgments

References

[1] Carpinelli J M, Weitering H H, Plummer E W and Stumpf R 1996 *Nature* **381** 398
[2] Carpinelli J M, Weitering H H, Bartkowiak M, Stumpf R and Plummer E W 1997 *Phys. Rev. Lett.* **79** 2859
[3] Melechko A V, Braun J, Weitering H H and Plummer E W 1999 *Phys. Rev. Lett.* **83** 999

[4]   Weitering H H, Carpinelli J M, Melechko A V, Zhang J, Bartkowiak M and Plummer E W 1999 *Science* **285** 2107

[5]   Zhang J, Ismail, Rous R J, Baddorf A P and Plummer E W 1999 *Phys. Rev.* B **60** 2860

[6]   Melechko A V, Braun J, Weitering H H and Plummer E W 2000 *Phys. Rev.* B **61** 2235

[7]   *Complex Systems—Science for the 21st Century (Report of a US Department of Energy, Office of Science Workshop) (Berkeley, CA, March 1999)*

[8]   Kidd T E, Miller T, Chou M Y and Chiang T-C 2000 *Phys. Rev. Lett.* **85** 3684

[9]   Okasinski J S, Walko D A, Kim C-Y and Bedzyk M J 2001 *Bull. Am. Phys. Soc.* **46** 374
      Okasinski J S, Walko D A, Kim C-Y and Bedzyk M J 2001 unpublished results presented orally

[10] Santoro G, Scandolo S and Tosatti E 1999 *Phys. Rev.* B **59** 1891

[11] Le Lay G, Aristov V Yu, Boström O, Layet J M, Asensio M C, Avila J, Huttel Y and Cricenti A 1998 *Appl. Surf. Sci.* **123/124** 440

[12] Goldoni A and Modesti S 1997 *Phys. Rev. Lett.* **79** 3266

[13] Uhrberg R I G and Balasubramanian T 1998 *Phys. Rev. Lett.* **81** 2108

[14] Avila J, Mascaraque A, Michel E G, Asensio M C, Le Lay G, Ortega J, Pérez R and Flores F 1999 *Phys. Rev. Lett.* **82** 442

[15] Avila J, Huttel Y, Le Lay G and Asensio M C 2000 *Appl. Surf. Sci.* **162+163** 48

[16] Asensio M C 2001 *Bull. Am. Phys. Soc.* **46** 849
      Asensio M C 2001 unpublished results presented orally
      Avila J, Mascaraque A, Le Lay G, Michel E G, Gothelid M, Ascolani H, Alvarez J, Ferrer S and Asensio M C *Preprint* unpublished

[17] Uhrberg R I G, Zhang H M and Balasubramanian T 2000 *Phys. Rev. Lett.* **85** 1036

[18] Gonzalez J 2000 *Phys. Rev.* B **62** 6928

[19] Flores F, Ortega J and Pérez R 1999 *Surf. Rev. Lett.* **6** 411

[20] Pérez R, Ortega J and Flores F 2000 *Appl. Surf. Sci.* **166** 45

[21] Ortega J, Pérez R and Flores F 2000 *J. Phys.: Condens. Matter* **12** L21

[22] Pérez R, Ortega J and Flores F 2001 *Phys. Rev. Lett.* **86** 4891

[23] Gor'kov L P and Grüner G (ed) 1989 *Charge Density Waves in Solids* (Amsterdam: Elsevier)

[24] Kidd T, Miller T and Chiang T-C 1999 *Phys. Rev. Lett.* **83** 2789
      Kidd T, Miller T and Chiang T-C 2000 *Phys. Rev. Lett.* **84** 3023

[25] Bunk O, Zeysing J H, Falkenberg G, Johnson R L, Nielsen M, Nielsen M M and Feidenhans'l R 1999 *Phys. Rev. Lett.* **83** 2226

[26] Petaccia L, Floreano L, Benes M, Cvetko D, Goldoni A, Grill L, Morgante A, Verdini A and Modesti S 2001 *Phys. Rev.* B **63** 115406

[27] Goshtasbi Rad M, Göthelid M, Le Lay G, Karlsson U O, Grehk T M and Sandell A 2001 *Surf. Sci.* **477** 227